PL-TR-97-2009

SURFACE TOPOGRAPHY EFFECTS ON Lg WAVE PROPAGATION IN HETEROGENEOUS CRUSTAL WAVEGUIDES

R. S. Wu
T. Lay
X. B. Xie
X. F. Chen

University of California/Santa Cruz
Institute of Tectonics
Santa Cruz, CA 95064

20 January 1997

Scientific Report No. 1

DEPARTMENT OF ENERGY
OFFICE OF NON-PROLIFERATION
AND NATIONAL SECURITY
WASHINGTON, DC 20585

PHILLIPS LABORATORY
Directorate of Geophysics
AIR FORCE MATERIEL COMMAND
HANSCOM AFB, MA 01731-3010

SPONSORED BY
Department of Energy
Office of Non-Proliferation and National Security

MONITORED BY
Phillips Laboratory
CONTRACT No. F19628-95-K-0016

This technical report has been reviewed and is approved for publication.

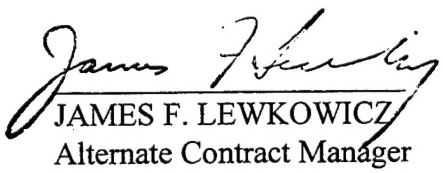

JAMES F. LEWKOWICZ
Alternate Contract Manager
Earth Sciences Division

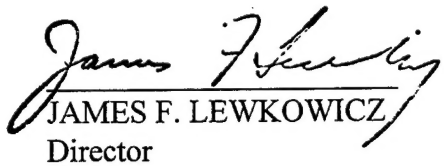

JAMES F. LEWKOWICZ
Director
Earth Sciences Division

This report has been reviewed by the ESD Public Affairs Office (PA) and is releasable to the National Technical Information Service (NTIS).

Qualified requestors may obtain copies from the Defense Technical Information Center. All others should apply to the National Technical Information Service.

If your address has changed, or you wish to be removed from the mailing list, or if the addressee is no longer employed by your organization, please notify PL/IM, 29 Randolph Road, Hanscom AFB, MA 01731-3010. This will assist us in maintaining a current mailing list.

Do not return copies of this report unless contractual obligations or notices on a specific document requires that it be returned.

REPORT DOCUMENTATION PAGE

Form Approved
OMB No. 0704-0188

1. AGENCY USE ONLY (Leave blank)	2. REPORT DATE	3. REPORT TYPE AND DATES COVERED
	20 January 1997	Scientific Report No. 1

4. TITLE AND SUBTITLE
Surface Topography Effects on Lg Wave Propagation in Heterogeneous Crustal Waveguides

5. FUNDING NUMBERS
PE 69120H
PR DENN TA GM WU AS

Contract F19628-95-K-0016

6. AUTHOR(S)
R. S. Wu
T. Lay
X. B. Xie
X. F. Chen

7. PERFORMING ORGANIZATION NAME(S) AND ADDRESS(ES)
University of California/Santa Cruz
Institute of Tectonics
Santa Cruz, CA 95064

8. PERFORMING ORGANIZATION REPORT NUMBER

9. SPONSORING / MONITORING AGENCY NAME(S) AND ADDRESS(ES)
Phillips Laboratory
29 Randolph Road
Hanscom AFB, MA 01731-3010

Contract Manager: James Lewkowicz/GPE

10. SPONSORING / MONITORING AGENCY REPORT NUMBER
PL-TR-97-2009

11. SUPPLEMENTARY NOTES
This research was sponsored by the Department of Energy, Office of Non-Proliferation and National Security, Washington, DC 20585

12a. DISTRIBUTION / AVAILABILITY STATEMENT
Approved for public release; distribution unlimited

12b. DISTRIBUTION CODE

13. ABSTRACT *(Maximum 200 words)*

The object of this research is to study the effects of surface topography, near-surface (sedimentary) structure and the associated small-scale heterogeneities on regional wave propagation which is critical for both discrimination and yield estimation in monitoring a Comprehensive Test Ban Treaty and the current Nuclear Non-Proliferation Treaty. We aim at developing a hybrid method which couples the recently developed fast screen propagator theory and methods (Wu, 1994; Wu and Xie, 1994; Wu and Huang, 1995) with a modified Boundary Integral Equation (BIE) method to treat the influences of both volume heterogeneities and irregular interfaces, including the influence of surface topography. We adopt Chen's Global Generalized Reflection/Transmission Matrix (GGRTM) method as the major element in our hybrid method. As the first step, we test both the generalized screen one-way wave method and the GGRTM method, and develop the connection of the two algorithms for the two-dimensional SH case. Chen's theory has been modified for this purpose and the connection formulas have been derived and numerically tested. The excellent agreement between seismograms for direct propagation and propagation using the connection formulas proves the correctness of the theory and the feasibility of the methodology.

14. SUBJECT TERMS			15. NUMBER OF PAGES
Seismic	Wave Propagation	Lg Wave	36
CTBT	Generalized Screen Method		16. PRICE CODE

17. SECURITY CLASSIFICATION OF REPORT	18. SECURITY CLASSIFICATION OF THIS PAGE	19. SECURITY CLASSIFICATION OF ABSTRACT	20. LIMITATION OF ABSTRACT
Unclassified	Unclassified	Unclassified	SAR

Contents

1 Introduction

The study of path effects of complex structure and heterogeneities on the excitation and propagation of regional phases in different areas remains critical for both discrimination and yield estimation procedures for monitoring the CTBT. The problem will be more severe in the case of Non-Proliferation monitoring, in which the potential nuclear tests may occur in very different geological and geophysical environments. Today, regional waves are one of the most important indicators for monitoring purpose. Due to the complexity involved in the regional phase propagation, synthetic simulation will play an important role in areas that lack enough data to rely on expirical methods. To meet these requirements, the ultimate goal is to develop a computationally viable technique for calculating high-frequency (1 - 25 Hz) synthetic seismograms in regional distance ($>$ 1000 km) for three dimensional, heterogeneous (on large and small scales) crustal structures including rough surface and interfaces.

In the past, boundary integral equation (BIE) or boundary element (BE) methods have been extensively used to study the effects of topography or sedimentary basin structures on ground motions at the surface. BE has been also used to study the Lg blockage problem with limited success. Blockage is assumed to be caused by coastlines, mountains and sudden change of crustal thickness. However, two-dimensional numerical simulations of blockage by large-scale crustal structures have not succeeded in matching the observations (Campillo et al., 1993; Gibson and Campillo, 1994). Most simulations are either for surface topography or for irregular structure beneath a flat surface (sedimentary layer) due to the restriction of computational complexity. However, the combination of both surface-topography and sedimentary structure may have more dramatic influence. An irregular surface and low-velocity layer can both trap part of the Lg energy into the surface layer and scatter the Lg wave out of the crustal waveguide. Existing methods are also not capable of simulating the combined effects of both large-scale structure and the associated small-scale heterogeneities. Irregular topography and near-surface structure are the manifestation of past and/or present tectonic processes which often produce crustal heterogeneities at different scales. The effects of the small-scale (wavelength-scale) heterogeneities must be taken into consideration in modeling blockage and other Lg propagation, scattering and attenuation phenomena.

We are developing a new hybrid numerical method by combining the generalized screen method with the boundary integral equation method. The generalized screen method can handle wave propagation in heterogeneous waveguide with modest topography. The method is based on one-way wave equation theory (Wu, 1994; 1996; Wu and Xie, 1994; Wu and Huang, 1995). In the crustal waveguide environment, major wave energy is carried by forward propagating waves, including forward scattered waves, and therefore the neglect of backscattered waves in the modeling will not change the main features of regional phases in most cases. By neglecting backscattering in the theory, the method becomes a forward marching algorithm in which the next step propagation depends only on the present value of wavefield in a transverse cross-section and the heterogeneities between the two cross-sections. The saving of computing time and storage is enormous. This makes it a very efficient method and can propagate high frequency regional signals to very long distances.

Modest surface topography can be modeled by coordinate transformation in the generalized screen method. The algorithm for handling the topography is still in the process of development. On the other hand, the boundary integral equation method has the flexibility to incorporate complex topographic features into the model. However, since matrix operations are involved, the boundary integral equation method is not efficient. When the ratio of model dimension to wavelength is too large, the computation time and memory requirement become formidable. This problem can be circumvented through a hybrid method. The hybrid method will combine the advantages of the above mentioned two methods and avoid their disadvantages. The Lg phases generated by the source are propagated to a certain distance with the generalized screen method. Then, the output will be used as the input to the boundary integral equation method, and the later is used to calculate the interaction between Lg wave and the complex waveguide structure with rough topographic features. This approach provide us a possibility to investigate the interaction between Lg wave and crustal waveguides having complicated structures including severe topography for long distance propagation.

As the first year's effort, the screen method has been successfully developed for a crustal waveguide for 2-D SH-wave propagation. The boundary integral equation method has been tested and connected to a laterally homogeneous crust model for 2-D SH-wave propagation. Numerical examples showed the feasibility of this approach. The next year's work will be to put

the topographic features into the hybrid method, and test the method for some realistic models, such as those for paths across the Tibet Plateau.

2 Generalized Screen Method

For an isotropic 2D elastic medium, the SH and the P-SV waves are decoupled. Here we treat only the SH problem to demonstrate the applicability of the screen propagators to crustal waveguide. Under such a circumstance, the equation of motion becomes

$$-\omega^2 \rho(\mathbf{r}) u(\mathbf{r}) = \frac{\partial}{\partial x}[\mu(\mathbf{r})\frac{\partial}{\partial x}u] + \frac{\partial}{\partial z}[\mu(\mathbf{r})\frac{\partial}{\partial z}u] \tag{1}$$

where ω is the frequency, $\mathbf{r} = (x, z)$ is a 2D position vector, u is transverse displacement, ρ is the density of the medium, and μ is the shear rigidity. We decompose the parameters of the elastic medium and the total wave field into

$$\begin{aligned} \rho &= \rho_0 + \delta\rho \\ \mu &= \mu_0 + \delta\mu \\ u &= u^0 + U \end{aligned} \tag{2}$$

where ρ_0 and μ_0 are parameters of the background medium, $\delta\rho$ and $\delta\mu$ are corresponding perturbations, u^0 is the primary field and U is the scattered field. Then, the SH wave equation can be rewritten as

$$\mu_0 \nabla^2 U + \omega^2 \rho_0 U = -[\omega^2 \delta\rho u + \nabla \cdot \delta\mu \nabla u] \,, \tag{3}$$

or

$$(\nabla^2 + k^2) U(\mathbf{r}) = -k^2 F(\mathbf{r}) u(\mathbf{r}) \,, \tag{4}$$

where $k = \omega/v$ is the wavenumber in the background medium and v is the background S wave velocity defined by

$$v = \sqrt{\mu_0/\rho_0} \tag{5}$$

In the right-hand side of (4), $F(\mathbf{r})$ is a perturbation operator

$$F(\mathbf{r}) = \varepsilon_\rho(\mathbf{r}) + \frac{1}{k^2}\nabla \cdot \varepsilon_\mu \nabla \,, \tag{6}$$

with

$$\varepsilon_\rho(\mathbf{r}) = \frac{\delta\rho(\mathbf{r})}{\rho_0}\,, \tag{7}$$

$$\varepsilon_\mu(\mathbf{r}) = \frac{\delta\mu(\mathbf{r})}{\mu_0}\,. \tag{8}$$

Equation (4) is a scalar Helmholtz equation. With a half-space scalar Green's function g^h, the scattered field U can be written as

$$U(\mathbf{r}_1) = k^2 \int_V d^2\mathbf{r} g^h(\mathbf{r}_1;\mathbf{r}) F(\mathbf{r}) u(\mathbf{r})\,, \tag{9}$$

where the 2D integration is over the volume V including all the heterogeneities in the modeling space. Under the forward-scattering approximation, the total field and Green's function under the integration in above equation can be replaced by their forward-scattering approximated counterparts, and the field can be calculated by a one-way marching algorithm along the x-direction using a dual domain technique.

2.1 Wide-angle Screen Approximation

The half-space model can be sliced into thin-slabs perpendicular to the propagation direction. Weak scattering condition holds for each thin-slab. For each forward step, the forward-scattered field by the thin-slab is calculated and added to the primary field so that the updated field becomes the incident field for the next thin-slab. The formulas of the dual-domain implementation are summarized as follows:

$$U(x_1, K_z) \;=\; U_\rho(x_1, K_z) + U_\mu(x_1, K_z) \tag{10}$$

where

$$U_\rho(x_1, K_z) = ik \int_{x'}^{x_1} dx e^{i\gamma(x_1 - x)} \mathcal{C}[\frac{k}{\gamma}\varepsilon_\rho(z) u_0(z)] \tag{11}$$

$$U_\mu(x_1, K_z) = ik \int_{x'}^{x_1} dx e^{i\gamma(x_1 - x)} \left\{ \mathcal{C}[\varepsilon_\mu(z)\bar{\partial}_x u_0(z)] - i\mathcal{S}[\frac{K_z}{\gamma}\varepsilon_\mu(z)\bar{\partial}_z u_0(z)] \right\} \tag{12}$$

where $\mathcal{C}[f(z)]$ and $\mathcal{S}[f(z)]$ are the cosine and sine transforms, defined by

$$\begin{aligned} \mathcal{C}[f(z)] &= \int_0^\infty dz 2\cos(K_z z) f(z) \\ \mathcal{S}[f(z)] &= \int_0^\infty dz 2\sin(K_z z) f(z) \end{aligned} \tag{13}$$

In Eq. (11) and (12), u_0, $\bar{\partial}_x u_0$ and $\bar{\partial}_z u_0$ can be calculated by

$$\begin{aligned} u_0(x,z) &= \frac{1}{2\pi}\int_{-\infty}^{\infty} dK_z' e^{iK_z' z} e^{i\gamma'(x-x')} u_0(x', K_z') \\ &= \mathcal{C}^{-1}[e^{i\gamma'(x-x')} u_0(x', K_z')] \end{aligned} \tag{14}$$

and

$$\begin{aligned} \bar{\partial}_x u_0(x,z) &= \mathcal{C}^{-1}[e^{i\gamma'(x-x')}\frac{\gamma'}{k} u_0(x', K_z')] \\ \bar{\partial}_z u_0(x,z) &= i\mathcal{S}^{-1}[e^{i\gamma'(x-x')}\frac{K_z'}{k} u_0(x', K_z')] \end{aligned} \tag{15}$$

Eq. (11), (12), (14) and (15) are the dual-domain expressions of the wide-angle screen propagator for half-space SH problems.

The procedure can be summarized as follows.

1. Cosine transform the incident fields at the entrance of each thin-slab into wavenumber domain.

2. Free propagate in wavenumber domain and calculate the primary field and its gradient within the slab.

3. At each horizontal position within the slab, inverse cosine/sine transform the primary field and its gradients into space domain and, then interact with the medium perturbations ε_ρ and ε_μ.

4. Cosine/sine transform the distorted fields into wavenumber domain and perform the divergence operations to get the scattered fields

5. Calculate the primary field at the slab exit and add to the scattered field to form the total field as the incident field at the entrance of the next thin-slab.

6. Continue the procedure iteratively.

2.2 Small Angle Screen Approximation and the Phase-Screen Propagator

When the energy of crustal guided waves are carried mainly by small-angle waves (with respect to the horizontal direction), the small angle approximations can be invoked to simplify the theory and calculations. Under the phase-screen approximation, the heterogeneous half-space is represented by a series of half-screens embedded in the homogeneous background half-space. The wave propagates between screens in the wavenumber domain and interacts with phase-screens in the space domain. The interaction is only a phase-delay operator (multiplication in space domain). The formula for dual-domain implementation is

$$\begin{aligned} u(x_1, K_z) &= u_0(x_1, K_z) + U(x_1, K_z) \\ &= e^{i\gamma(x_1 - x')} \int_0^\infty dz 2\cos(K_z z)[1 + ik2S_s(z)]u_0(x', z) \\ &\approx e^{i\gamma(x_1 - x')} \mathcal{C}\left[e^{2ikS_s(z)} u_0(x', z)\right] \end{aligned} \tag{16}$$

where $exp[2ikS_s(z)]$ is the phase delay operator. The procedure can be summarized as follows.

1. Cosine transform the incident field at the starting plane into wavenumber domain and free propagate to the screen.

2. Inverse cosine transform the incident field into space domain and interact with the shear slowness screen (phase-screen) to get the transmitted field.

3. Cosine transform the transmitted field into wavenumber domain and free propagate to the next screen.

4. Repeat the propagation and interaction screen-by-screen to the boundary of the model space.

2.3 Treatment of the Moho Discontinuity

The Moho discontinuity can be treated in two ways. One is to put the impedance boundary conditions in the formulation, the other is to treat the parameter changes as perturbations and therefore be incorporated into the screen interaction. The former has the advantage of computational efficiency. The latter has the flexibility of handling irregular interfaces. Here, we adopt

the latter approach and check the validity of the perturbation approach for the Moho discontinuity by a reflectivity method and a finite difference algorithm.

3 Global Generalized Reflection Transmission Matrix Method

The discretization of BIE can be done by integration of the Green's function either in space domain (e.g. Sanches-Sesma and Campillo, 1991), or in wavenumber domain using the discrete wave number representation (Bouchon, 1985; Campillo and Bouchon, 1985; Chen, 1990, 1995, 1996). In the latter approach, the singularity problem of the Green's function is avoided by using truncated series. The wavenumber domain BIE has another advantage that it can be easily extended to the case of multilayered media with irregular interfaces. In Bouchon et al. (1989), propagator matrices are used to relate equivalent force distributions on neighboring interfaces. Chen (1990, 1995, 1996) related the fields at neighboring layers by global reflection/transmission coefficients and then derived the global generalized R/T coefficients to relate observations and sources. In these methods, the dimensionality of the linear system to solve are independent of the number of layers involved. The computation time increases only linearly with the number of interfaces. For this reason, we adopt Chen's GGRTM (Global Generalized Reflection/Transmission Matrix) method as the candidate in our hybrid method.

The GGRTM can be viewed as an extension of the reflectivity method for horizontally layered case to an irregularly layered case, and it has been demonstrated to be an accurate and effective method to simulate seismic waves in laterally varying layered media (Chen, 1991, 1995, 1996). For example, for the scattering problem due to a semi-circular canyon (shown in Figure 1), GGRTM can provide very accurate results. Figures 2 and 3 show the comparisons of the results (solid lines) computed by GGRTM with the analytical solutions of Trifunac (dotted lines) for various normalized frequencies, showing excellent agreement between them. It is known that in this semi-circular canyon model, there are two sharp edges. Many other methods, e.g., Aki-Larner method, T-matrix method and other high-frequency

asymptotic methods, fail to provide correct solutions.

3.1 Connection Formulation

Assume domain II is the model space we are interested in and the field in domain I is easy to calculate by other less expensive methods. According to the representation theorem, wave-fields inside domain II can be expressed as

$$u^{II}(\mathbf{x},\omega) = \int_0^{+\infty} \left\{ \tau^I(\mathbf{x}') + u^I(\mathbf{x}')\mu(z')\frac{\partial}{\partial x'} \right\} G^{II}(\mathbf{x},\mathbf{x}')dz' \qquad (17)$$

Where u^I and τ^I are the displacement and traction fields on the vertical boundary surface dividing domain I and II, and can be calculated using methods valid in domain I, μ is the shear rigidity, and G^{II} is the Green's function in domain II which will be calculated by GGRTM.

3.2 Algorithm of Computing Synthetic Lg Waves

Having the connection formulation, we can use GGRTM to compute synthetic Lg waves. The step-by-step procedure of applying GGRTM to computing a synthetic seismogram in a general irregularly layered medium can be summarized as follows.

Step 1

Calculate the interface matrices for each interface, $\mathbf{Q}^{(j)}_{\downarrow\uparrow}$, $\mathbf{Q}^{(j)}_{\uparrow\downarrow}$, $\mathbf{Q}^{(j)}_{\uparrow\uparrow}$, $\mathbf{Q}^{(j)}_{\downarrow\downarrow}$, $\mathbf{P}^{(j)}_{\uparrow\uparrow}$, $\mathbf{P}^{(j)}_{\downarrow\downarrow}$, $\mathbf{P}^{(j)}_{\uparrow\downarrow}$, $\mathbf{P}^{(j)}_{\downarrow\uparrow}$; for j=1,2, ..., N, by carrying out the integrals over each interface. These interface matrices contain the structural information of the media and are defined as (Chen, 1990)

$$\left(\mathbf{Q}^{(j)}_{\downarrow\uparrow}\right)_n = \frac{-1}{2\nu_n^{(j)}L} \int_{-L/2}^{L/2} \left\{ \dot{\xi}^{(j-1)}(x)k_n + \nu_n^{(j)} \right\} \exp[i\Xi^{(j)}_{\downarrow\uparrow}(x,n,m)]dx \,, \qquad (18)$$

$$\left(\mathbf{Q}^{(j)}_{\downarrow\downarrow}\right)_n = \frac{-1}{2\nu_n^{(j)}L} \int_{-L/2}^{L/2} \left\{ \dot{\xi}^{(j-1)}(x)k_n - \nu_n^{(j)} \right\} \exp[i\Xi^{(j)}_{\downarrow\downarrow}(x,n,m)]dx \,, \qquad (19)$$

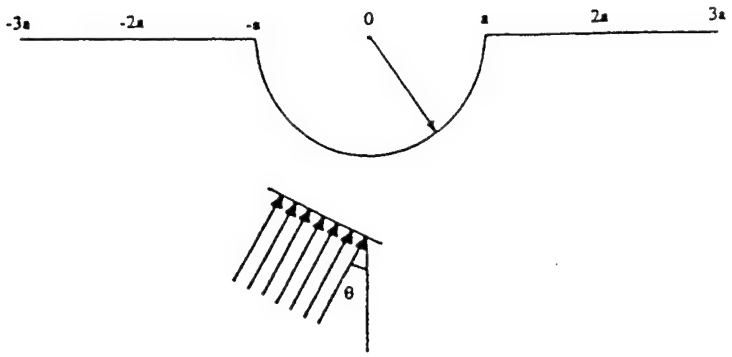

Figure 1: The configuration of the scattering problem due to a semi-circular canyon and an incident plane wave, where a is the radius of the canyon, and θ is the angle of incident wave.

$$\left(\mathbf{Q}_{\uparrow\downarrow}^{(j)}\right)_n = \frac{-1}{2\nu_n^{(j)}L}\int_{-L/2}^{L/2}\left\{\dot{\xi}^{(j)}(x)k_n - \nu_n^{(j)}\right\}\exp[i\Xi_{\uparrow\downarrow}^{(j)}(x,n,m)]dx\,, \tag{20}$$

$$\left(\mathbf{Q}_{\uparrow\uparrow}^{(j)}\right)_n = \frac{-1}{2\nu_n^{(j)}L}\int_{-L/2}^{L/2}\left\{\dot{\xi}^{(j)}(x)k_n + \nu_n^{(j)}\right\}\exp[i\Xi_{\uparrow\uparrow}^{(j)}(x,n,m)]dx\,, \tag{21}$$

$$\left(\mathbf{P}_{\downarrow\uparrow}^{(j)}\right)_n = \frac{-\nu_m^{(j)}}{2\nu_n^{(j)}L}\int_{-L/2}^{L/2}\left\{1+[\dot{\xi}^{(j-1)}(x)]^2\right\}^{12}\exp[i\Xi_{\downarrow\uparrow}^{(j)}(x,n,m)]dx\,, \tag{22}$$

$$\left(\mathbf{P}_{\downarrow\downarrow}^{(j)}\right)_n = \frac{-\nu_m^{(j)}}{2\nu_n^{(j)}L}\int_{-L/2}^{L/2}\left\{1+[\dot{\xi}^{(j-1)}(x)]^2\right\}^{12}\exp[i\Xi_{\downarrow\downarrow}^{(j)}(x,n,m)]dx\,, \tag{23}$$

$$\left(\mathbf{P}_{\uparrow\downarrow}^{(j)}\right)_n = \frac{-\mu^{(j+1)}\nu_m^{(j+1)}}{2\mu^{(j)}\nu_n^{(j)}L}\int_{-L/2}^{L/2}\left\{1+[\dot{\xi}^{(j)}(x)]^2\right\}^{12}\exp[i\Xi_{\uparrow\downarrow}^{(j)}(x,n,m)]dx\,, \tag{24}$$

and

$$\left(\mathbf{P}_{\uparrow\uparrow}^{(j)}\right)_n = \frac{-\mu^{(j+1)}\nu_m^{(j+1)}}{2\mu^{(j)}\nu_n^{(j)}L}\int_{-L/2}^{L/2}\left\{1+[\dot{\xi}^{(j)}(x)]^2\right\}^{12}\exp[i\Xi_{\uparrow\uparrow}^{(j)}(x,n,m)]dx\,, \tag{25}$$

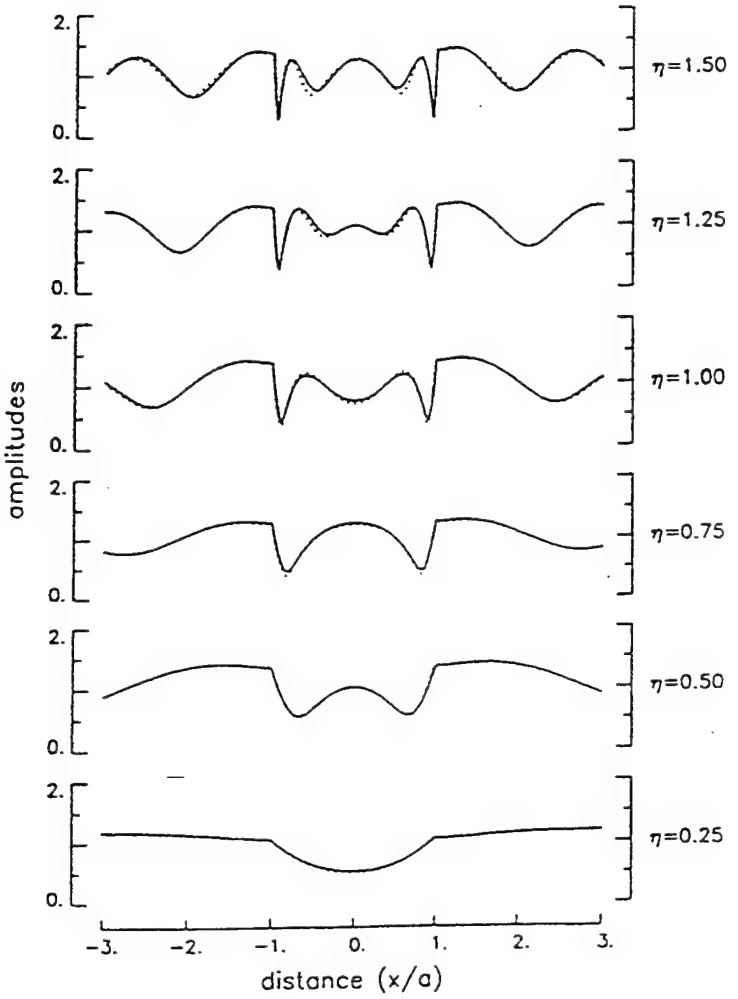

Figure 2: The frequency responses of a semi-circular canyon to vertical incident SH-wave for various normalized frequencies. The solid lines denote our results and the dotted lines denote the exact solutions.

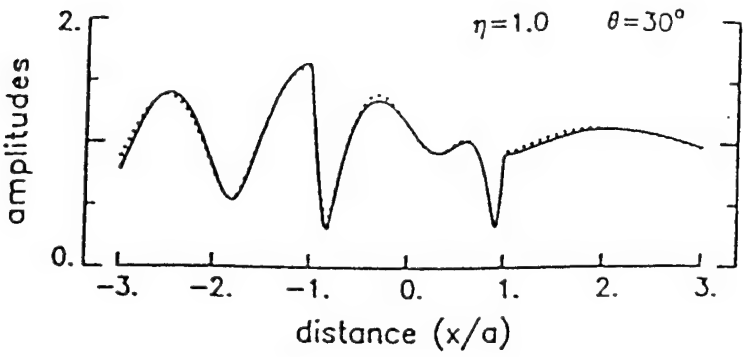

Figure 3: The same response as Figure 2, except that the incident angle is 30^o.

where $\xi^{(j)}(x)$ is the height of the topography for the jth interface, and

$$k_n = 2\pi nL \;\; \nu_n^{(j)} = \sqrt{(\omega\beta^{(j)})^2 - (k_n)^2} \;\; , \text{ and } \mathrm{Im}\left\{\nu_n^{(j)}\right\} \geq 0,$$

$$\Xi_{\uparrow\uparrow}^{(j)}(x,n,m) = (k_m - k_n)x + \nu_n^{(j)}[\xi^{(j)}(x) - \xi_{\min}^{(j)}] + \nu_m^{(j+1)} \left|\Delta\xi^{(j)}(x)\right| \;\; ,$$

$$\Xi_{\downarrow\uparrow}^{(j)}(x,n,m) = (k_m - k_n)x + \nu_n^{(j)}[\xi^{(j-1)}(x) - \xi_{\min}^{(j-1)}] + \nu_m^{(j)} \left|\Delta\xi^{(j-1)}(x)\right| \;\; ,$$

and

$$\Xi_{\downarrow\downarrow}^{(j)}(x,n,m) = (k_m - k_n)x - \nu_n^{(j)}[\xi^{(j-1)}(x) - \xi_{\max}^{(j-1)}] + \nu_m^{(j)} \left|\Delta\xi^{(j-1)}(x)\right| \;\; ;$$

for j = 1, 2, ..., N.

Where $\Delta\xi^{(j)}(x) = \xi^{(j)}(x) - z^{(j)}$.

Step 2

Calculate the global modified reflection and/or transmission matrices, { $\mathbf{R}_{\downarrow\uparrow}^{(j)}$ $\mathbf{T}_{\uparrow\uparrow}^{(j)}$ $\mathbf{T}_{\downarrow\downarrow}^{(j)}$ $\mathbf{R}_{\uparrow\downarrow}^{(j)}$ }, from the interface matrices using the following formulas:

$$\begin{bmatrix} \mathbf{R}_{\downarrow\uparrow}^{(j)} & \mathbf{T}_{\uparrow\uparrow}^{(j)} \\ \mathbf{T}_{\downarrow\downarrow}^{(j)} & \mathbf{R}_{\uparrow\downarrow}^{(j)} \end{bmatrix} = \begin{bmatrix} \mathbf{Q}_{\uparrow\uparrow}^{(j)} & \mathbf{P}_{\uparrow\uparrow}^{(j)} \\ -\mathbf{Q}_{\downarrow\downarrow}^{(j+1)} & -\mathbf{P}_{\downarrow\downarrow}^{(j+1)} \end{bmatrix} \begin{bmatrix} -\mathbf{Q}_{\uparrow\downarrow}^{(j)} & -\mathbf{P}_{\uparrow\downarrow}^{(j)} \\ \mathbf{Q}_{\downarrow\uparrow}^{(j+1)} & \mathbf{P}_{\downarrow\uparrow}^{(j+1)} \end{bmatrix}^{-1} \begin{bmatrix} \mathbf{E}_{\max}^{(j)} & \\ & \mathbf{E}_{\min}^{(j+1)} \end{bmatrix} , \tag{26}$$

and

$$\mathbf{R}_{\uparrow\downarrow}^{(o)} = -\mathbf{Q}_{\downarrow\downarrow}^{(1)} \left(\mathbf{Q}_{\downarrow\uparrow}^{(1)}\right)^{-1} \mathbf{E}_{\min}^{(1)} , \tag{27}$$

Where $\mathbf{E}_{\min}^{(j)}$ and $\mathbf{E}_{\max}^{(j)}$ are diagonal matrices given by

$$\mathbf{E}_{\min}^{(j)} = diagonal \left\{ \exp[iv_n^{(j)}(\xi_{\min}^{(j)} - \xi_{\min}^{(j-1)})];\ n = 0, \pm 1, \pm 2, ... \right\},$$

and

$$\mathbf{E}_{\max}^{(j)} = diagonal \left\{ \exp[iv_n^{(j)}(\xi_{\max}^{(j)} - \xi_{\max}^{(j-1)})];\ n = 0, \pm 1, \pm 2, ... \right\}.$$

These global modified reflection and/or transmission matrices describe the reflection and/or transmission effects due to single interface regardless of the influences from other existing interfaces.

Step 3

Compute the global generalized reflection and/or transmission matrices, $\hat{\mathbf{T}}_{\uparrow\uparrow}^{(j)}$, $\hat{\mathbf{R}}_{\downarrow\uparrow}^{(j)}$, $\hat{\mathbf{T}}_{\downarrow\downarrow}^{(j)}$, and $\hat{\mathbf{R}}_{\uparrow\downarrow}^{(j)}$, from the global modified reflection and/or transmission matrices through following recursive formulas:

$$\begin{aligned} \hat{\mathbf{R}}_{\uparrow\downarrow}^{(o)} &= \mathbf{R}_{\uparrow\downarrow}^{(o)} \\ \hat{\mathbf{T}}_{\uparrow\uparrow}^{(j)} &= [\mathbf{I} - \hat{\mathbf{R}}_{\downarrow\uparrow}^{(j)} \hat{\mathbf{R}}_{\uparrow\downarrow}^{(j-1)}]^{-1} \mathbf{T}_{\uparrow\uparrow}^{(j)} , \quad for\ j = 1, 2, ..., N; \\ \hat{\mathbf{R}}_{\downarrow\uparrow}^{(j)} &= \mathbf{R}_{\downarrow\uparrow}^{(j)} + \mathbf{T}_{\downarrow\downarrow}^{(j)} \hat{\mathbf{R}}_{\uparrow\downarrow}^{(j-1)} \hat{\mathbf{T}}_{\uparrow\uparrow}^{(j)} \end{aligned} \tag{28}$$

and

$$\begin{aligned} \hat{\mathbf{R}}_{\downarrow\uparrow}^{(N+1)} &= 0 \\ \hat{\mathbf{T}}_{\downarrow\downarrow}^{(j)} &= [\mathbf{I} - \hat{\mathbf{R}}_{\uparrow\downarrow}^{(j)} \hat{\mathbf{R}}_{\downarrow\uparrow}^{(j+1)}]^{-1} \mathbf{T}_{\downarrow\downarrow}^{(j)} , \quad for\ j = N, N-1, ..., 2, 1. \\ \hat{\mathbf{R}}_{\uparrow\downarrow}^{(j)} &= \mathbf{R}_{\uparrow\downarrow}^{(j)} + \mathbf{T}_{\uparrow\uparrow}^{(j)} \hat{\mathbf{R}}_{\downarrow\uparrow}^{(j+1)} \hat{\mathbf{T}}_{\downarrow\downarrow}^{(j)} \end{aligned} \tag{29}$$

These global generalized reflection and/or transmission matrices represent the total reflection and/or transmissions due to the multi-irregular layers.

Step 4

Compute the expansion coefficients of displacement spectra at free surface,

$$z = \xi^{(0)}(x),$$

by using the formula

$$\underline{\alpha}^{(o)} = \left(\mathbf{Q}_{\downarrow\uparrow}^{(1)}\right)^{-1} \mathbf{E}_{\min}^{(1)} \left\{\hat{\mathbf{s}}_{\uparrow}^{(1)} + \hat{\mathbf{T}}_{\uparrow\uparrow}^{(1)}\hat{\mathbf{s}}_{\uparrow}^{(2)} + \hat{\mathbf{T}}_{\uparrow\uparrow}^{(1)}\hat{\mathbf{T}}_{\uparrow\uparrow}^{(2)}\hat{\mathbf{s}}_{\uparrow}^{(3)} + \ldots + \hat{\mathbf{T}}_{\uparrow\uparrow}^{(1)}\hat{\mathbf{T}}_{\uparrow\uparrow}^{(2)}\ldots\hat{\mathbf{T}}_{\uparrow\uparrow}^{(N)}\hat{\mathbf{s}}_{\uparrow}^{(N+1)}\right\} , \tag{30}$$

where $\hat{\mathbf{s}}_{\uparrow}^{(j)}$ is the equivalent source term for the jth layer derived by the representation theorem and

$$\hat{\mathbf{s}}_{\uparrow}^{(j)} = \left\{\mathbf{I} - \hat{\mathbf{R}}_{\uparrow\downarrow}^{(j-1)}\hat{\mathbf{R}}_{\downarrow\uparrow}^{(j)}\right\}^{-1} \left(\mathbf{s}_{\uparrow}^{(j)} + \hat{\mathbf{R}}_{\downarrow\uparrow}^{(j)}\mathbf{s}_{\downarrow}^{(j)}\right) , \tag{31}$$

$$\left(\mathbf{s}_{\uparrow}^{(j)}\right)_n = \frac{i}{2\nu_n^{(s)}L} \int_{-L/2}^{L/2} dx \int_{\xi^{(j-1)}(x)}^{\xi^{(j)}(x)} f^{(j)}(x,z) \exp[-ik_n x + i\nu_n^{(j)}(z - \xi_{\min}^{(j)})]dz , \tag{32}$$

$$\left(\mathbf{s}_{\downarrow}^{(j)}\right)_n = \frac{i}{2\nu_n^{(j)}L} \int_{-L/2}^{L/2} dx \int_{\xi^{(j-1)}(x)}^{\xi^{(j)}(x)} f^{(j)}(x,z) \exp[-ik_n x - i\nu_n^{(j)}(z - \xi_{\max}^{(j-1)})]dz , \tag{33}$$

for j =1, 2, ..., N, N+1;

and

$$f^{(j)}(x,z) = \left\{\tau^{(j)}(x,z) + \mu^{(j)}u^{(j)}(x,z)\frac{\partial}{\partial x}\right\} . \tag{34}$$

Step 5

Calculate the displacement spectra at the free surface by using the following formula:

$$W^{(o)}[x, \xi^{(o)}(x), \omega] = \sum_{m=-M}^{M} \alpha_m^{(o)} \exp\left\{ik_m + i\nu_m^{(1)}\left|\Delta\xi^{(o)}(x)\right|\right\} . \tag{35}$$

Taking the Fourier transform on the above frequency domain solution, we can finally obtain the time domain solution, i.e., the synthetic seismogram.

4 Numerical Simulations

4.1 Numerical Simulations for Screen Method

In this section, we give examples of using the half-space phase-screen algorithm for regional wave propagation. First, in Figure 4 we show the accuracy of the method by comparing the synthetic seismograms generated by the screen method (thick lines) with those calculated by a reflectivity method (thin lines) for a flat crustal model. The crust has a thickness of 32 km and a shear wave velocity of 3.5 km/s. The mantle beneath the crust has a shear velocity of 4.5 km/s. The source function is a Ricker wavelet with a dominant frequency of 1.0 Hz. Except for near vertical reflections, where one way wave equation methods have difficulty, the results show excellent agreement. For long distance regional waves, the contribution of near vertical reflections is negligible. Next, we show the accuracy of the method by comparing synthetic seismograms generated by this method with those generated by a finite difference algorithm (Xie and Lay, 1994). For the finite-difference method, a fourth-order elastic SH-wave code is used to calculate the synthetic seismograms. The spatial sampling interval is 0.125 km and the time interval is 0.015 *second*. For the screen method, the spatial sampling interval is 0.25 km in vertical direction and the screen interval is 1.0 km. A Gaussian derivative is used as the source time function for both methods. Because of the computational intensity of the finite difference method, we did the comparison at short propagation distances. Shown on the top of Figure 5 is the crust model used to calculate synthetic seismograms; on the bottom, synthetic seismograms along a vertical profile at an epicenter distance of 250 km. The thin lines are from the finite difference method and the thick lines are from the generalized screen method. The source is located at a depth of 2 km. Excellent agreement can be seen.

Figure 6 shows the snap shots from the Screen method at 50 *sec.* for flat, narrowing and broadening crustal waveguides (from top to bottom, respectively). The source is located at the top-left corner at depth 2 km. The development of mantle wave and head wave, and the formation of crust guided wave as multiple reflections between the free surface and Moho discontinuity can be clearly seen. For the inhomogeneous models, wave diffraction, leakage to the mantle, wavefront distortion and increase of wavefield complexity can be also seen clearly. From the comparison it is seen that the passage of narrow

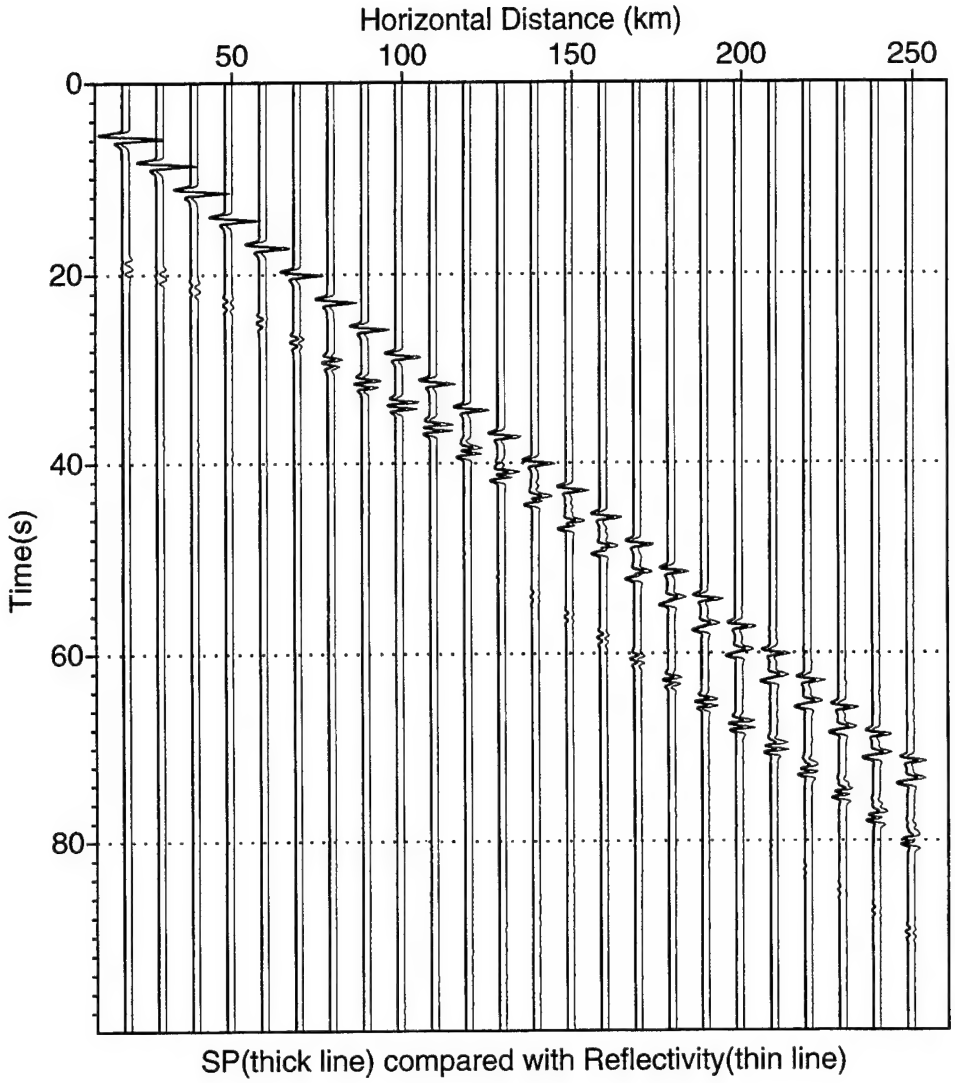

Figure 4: Comparison of synthetic seismograms along the surface calculated by the screen method and reflectivity method for a flat crustal model (32 km thick). The source function is a Ricker wavelet with dominant frequency of 1.0 Hz.

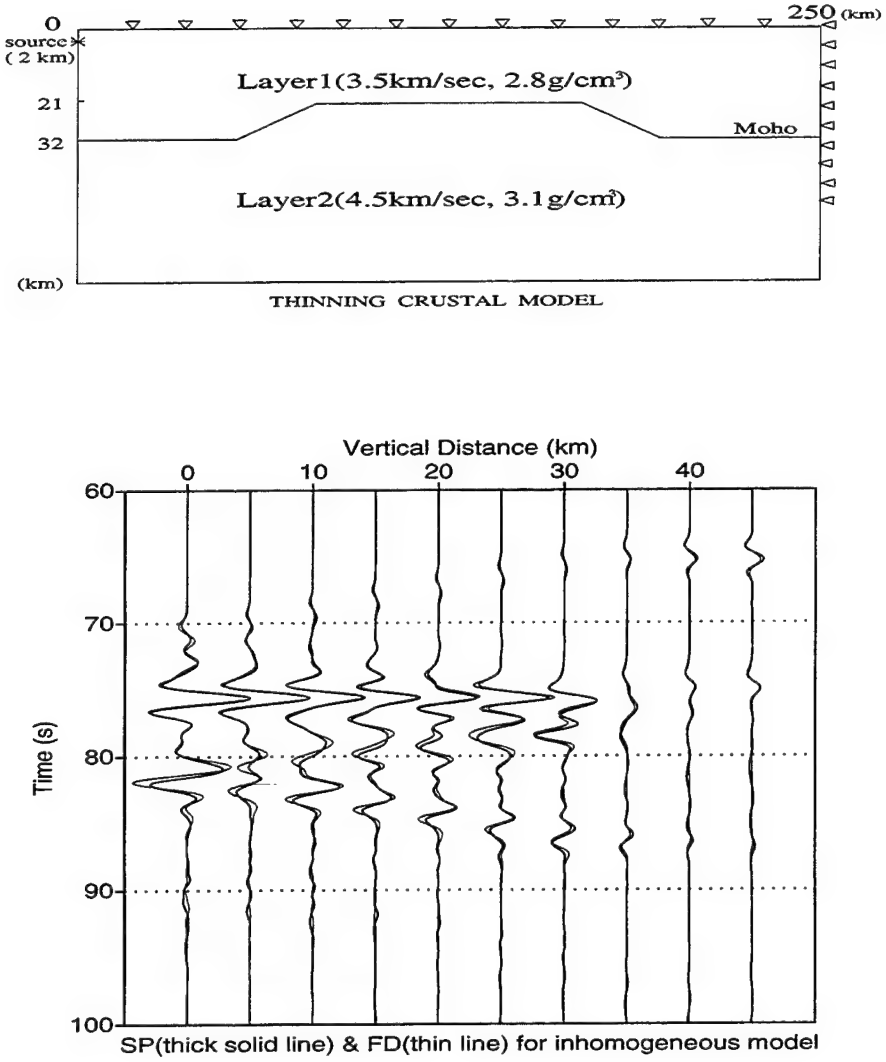

Figure 5: Comparison of synthetic seismograms along a vertical profile at the distance of 250 km calculated by the screen method (thick lines) and a finite-difference method (thin lines) for a laterally varying crustal model shown on the top panel.

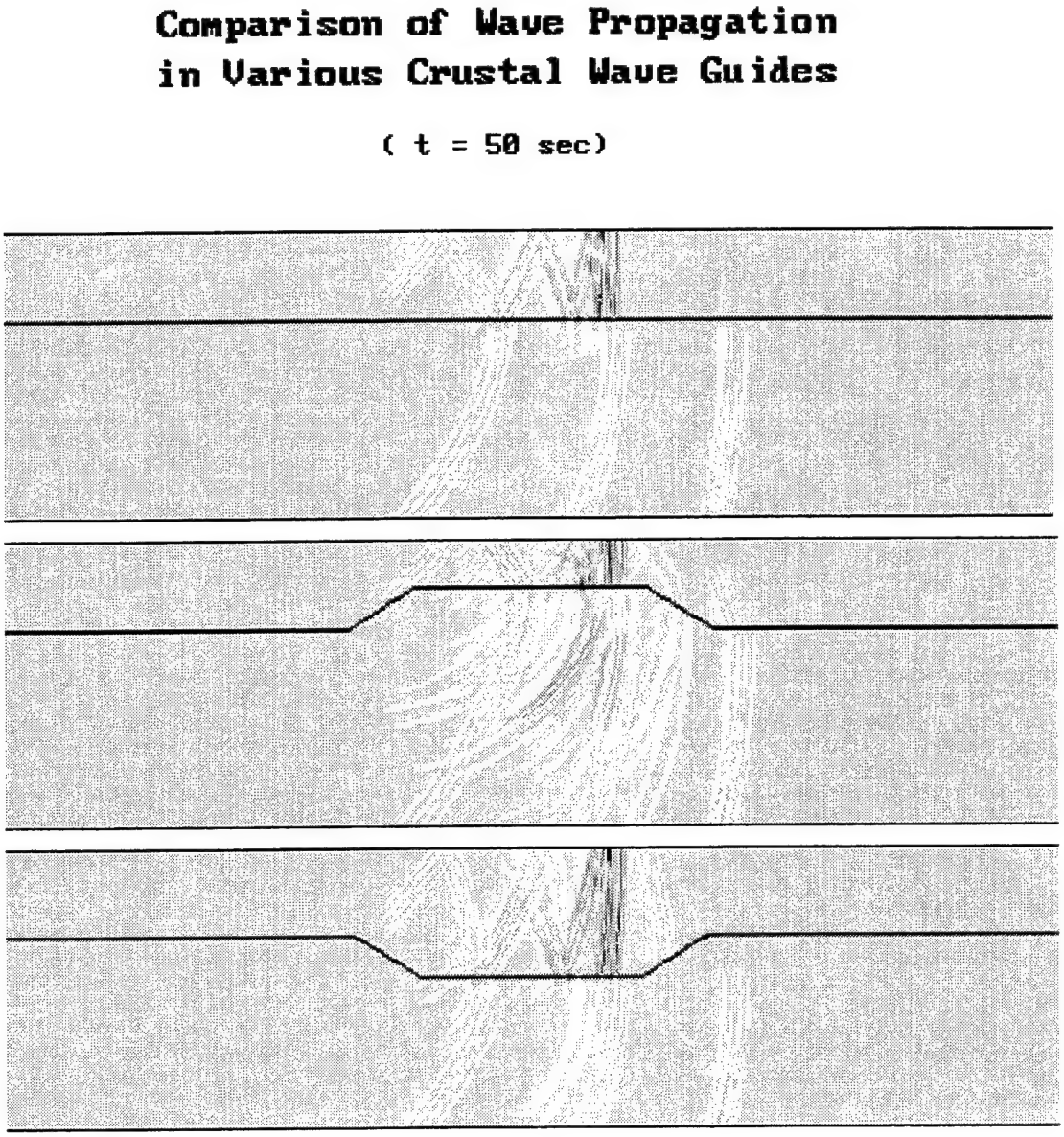

Figure 6: Snap shots at 50 *sec.* for various crustal waveguides.

crustal waveguide has greater effect on Lg leakage than the broad passage. In the latter case although the wavefronts are complicated due to scattering at the edges, most of the energy is still trapped in the crust, different from the case of a narrow passage in which a large percentage of energy leaks into the mantle. This example demonstrates the potential of the method as a tool for investigating the path effects of different crustal structures.

Figure 7 shows the synthetic seismograms by the screen method for the Flora-Asnes crust model in the NORSAR region. The parameters for this model are listed in Table 1. The model has a low velocity top layer 1 km thick and a velocity discontinuity at depth 15 km. The receivers are on the surface. A Ricker wavelet is used for this simulation with $f_0 = 1\ Hz$. Shown in the upper panel are short distances (up to 350 km); the lower panel shows long distances (up to 1000 km). In this case the Lg group is formed by multiple reflections of the Moho and the crustal discontinuities, complicated by the low velocity sedimental layer.

Table 1: Flora-Asnes crust model

thickness (km)	V_s (km/s)	ρ (g/cm^3)
1.00	3.00	2.60
14.00	3.46	2.80
22.00	3.76	3.00
infinity	4.65	3.30

The following example shows the potential capability of this method for long distance high-frequency synthetic seismograms in a laterally varying structure. Figure 8 shows the laterally varying crust model used in the calculation. Figure 9 shows the high-frequency synthetic seismograms on the surface at distances up to 1000 km. The center frequency is 5 Hz with the maximum frequency of 10 Hz. In comparison, the low-frequency ($f_c =$ 1 Hz, $f_{max} = 2$ Hz) synthetic seismograms are shown in Figure 10. It is clear that without high-frequency content, many of the distinctive features associated with Lg measurements can not be adequately modeled. In other words, a proper simulation method with the capability to generate accurate high-frequency signals is a necessity for the purpose of investigating regional phases. The generalized screen method with its high efficiency serves well as an important element of the hybrid method.

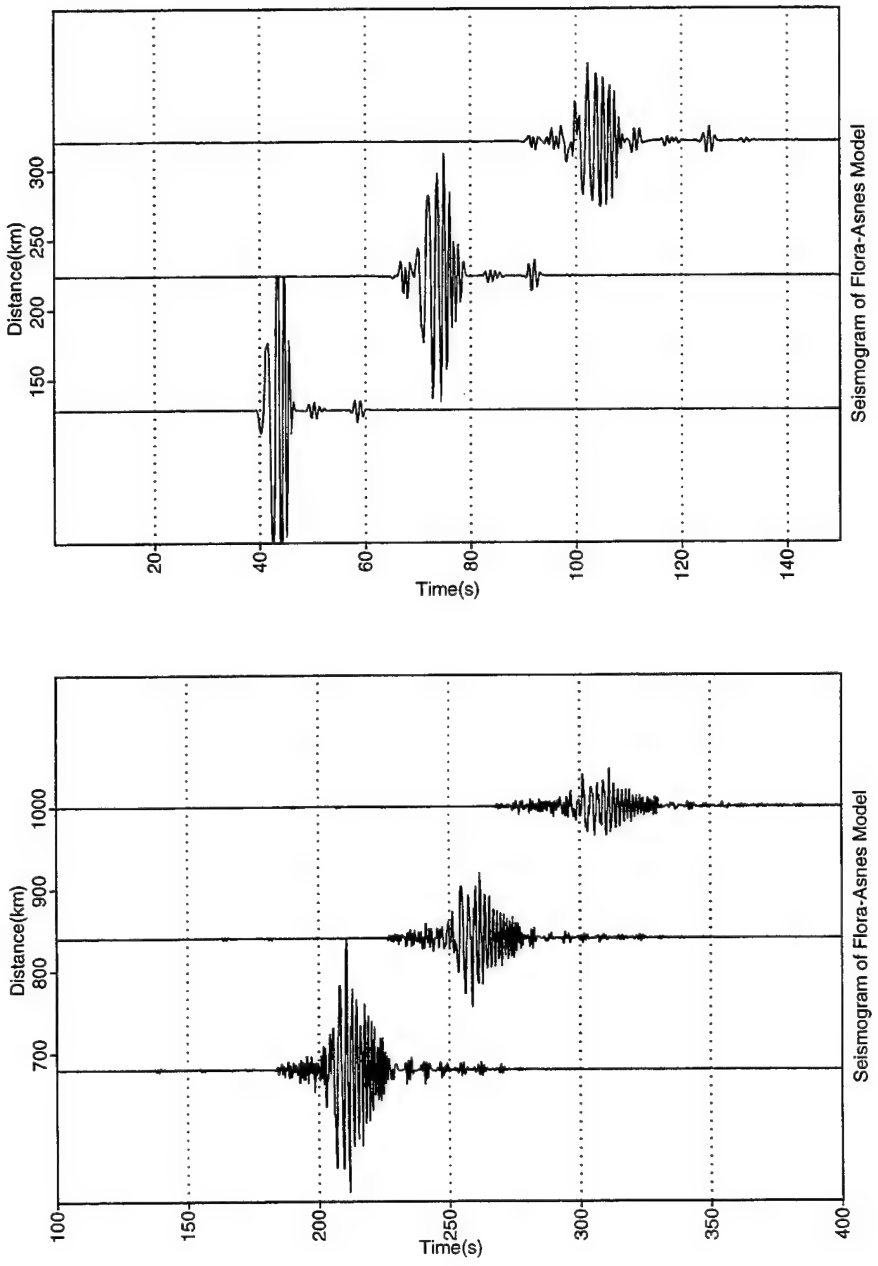

Figure 7: synthetic seismograms for the Flora-Asnes crust model in the NORSAR region. The parameters for this model are listed in Table 1.

Parameters of Crustal Model

Layer	Vs(km/sec)	Density(g/cm)	Thickness(km)
1	3.00	2.60	1.00
2	3.46	2.80	14.00
3	3.76	3.00	22.00
4	4.65	3.30	Half-Space

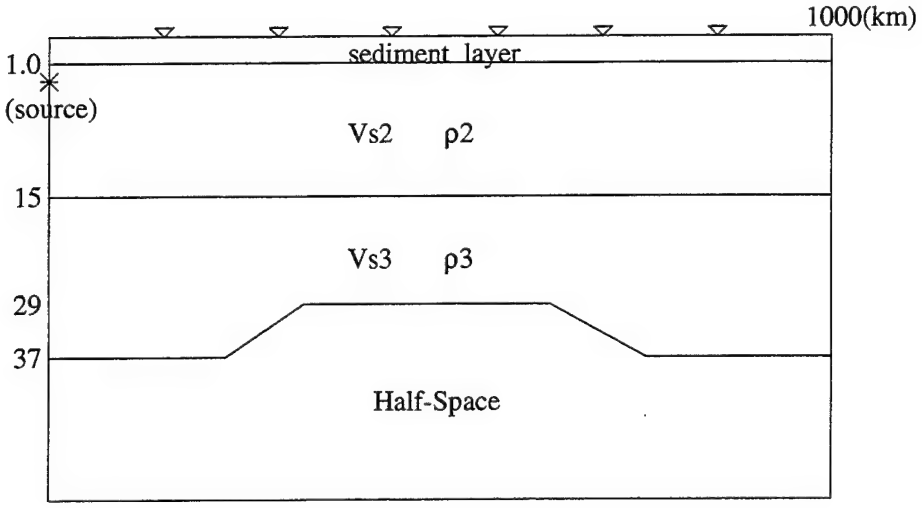

Crustal Model

Figure 8: An inhomogeneous crustal model used in the calculation of h-f synthetic seismograms. Shown in the upper panel are model parameters and the lower panel gives the geometry of the model. The receivers are on the surface and shown by triangles.

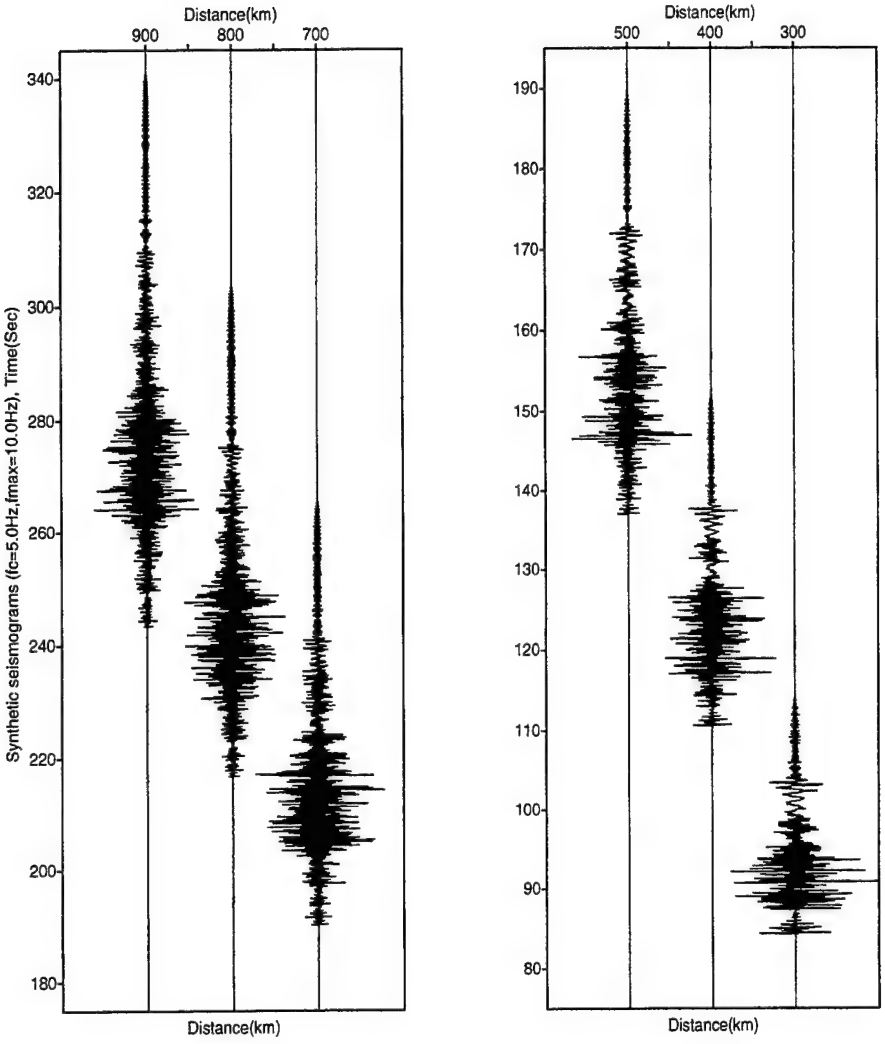

Figure 9: High-frequency ($f_c = 5$ Hz, $f_{max} = 10$ Hz) synthetic seismograms on the surface at distances up to 1000 km for an inhomogeneous crustal waveguide (Figure 8).

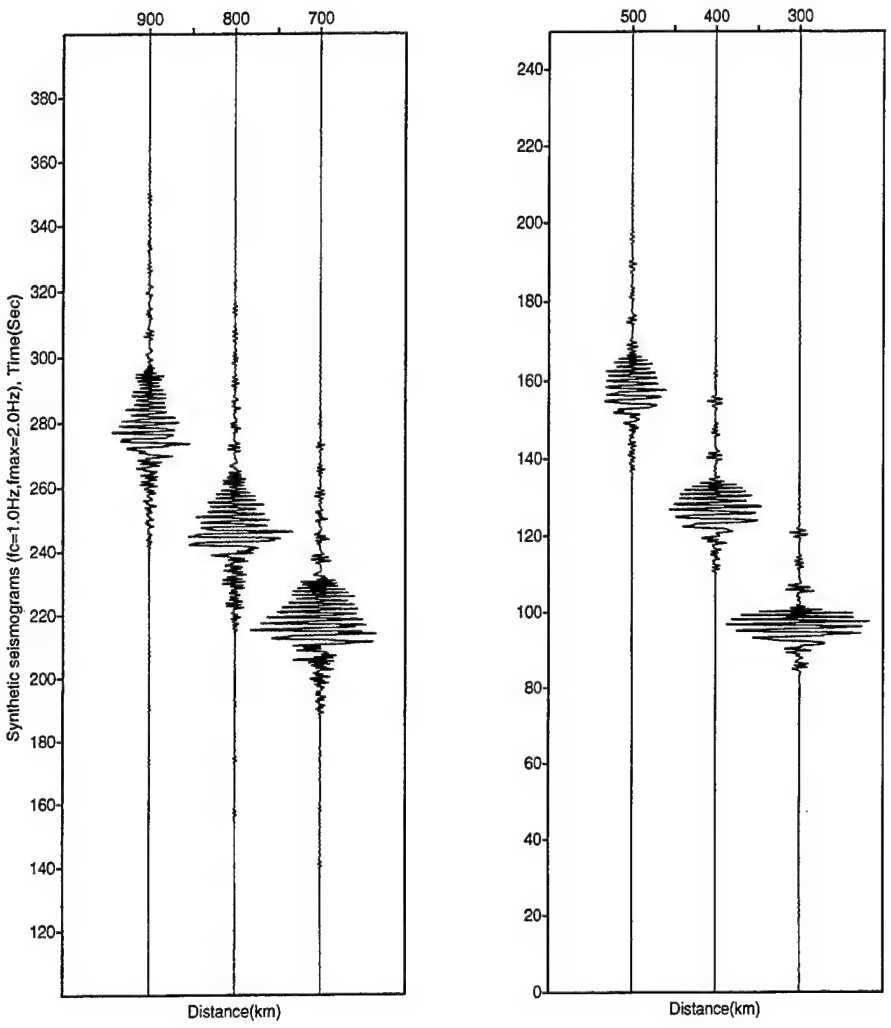

Figure 10: low-frequency ($f_c = 1$ Hz, $f_{max} = 2$ Hz) synthetic seismograms on the surface at distances up to 1000 km for an inhomogeneous crustal waveguide (Figure 8).

4.2 Numerical Test for BIE Method

To test the validity of our hybrid method, we consider a trivial case: a laterally homogeneous layered model. This problem can be fully solved by reflectivity method. To test our algorithm, we use our hybrid method to synthesize the seismograms, then check the results with the reflectivity method. The test model is a single layer crustal model. The velocities and densities of the crust and mantle are 3.5 km/sec, 2.8 g/cm^3, 4.5 km/sec and 3.2 g/cm^3 , respectively. The thickness of the crust is 32 km, seismic source is buried at z_s=2 km and x_s=0 km. Receiver is placed at z_0=0 km and x_0=250 km. The connection boundary is located at x=150 km. The synthetic seismogram of reflectivity method is plotted in Figure 11a and the synthetic seismogram from GGRTM is shown in Figure 11b. Comparison of these two seismograms shows an excellent agreement, confirming the validity of the connection scheme for our hybrid method.

The computer code for calculating general irregular media is under development at this stage, and expected to be finished soon. We will then calculate synthetic Lg waves propagating through an arbitrarily irregular layered medium to study the influence of surface topography and interface irregularities.

5 Conclusion and Discussions

We have derived the connection formulas for our hybrid scheme and its validity has been proved by numerical tests. Both generalized screen method and boundary integral equation method have been tested for the waveguide environment. The algorithm for seismogram synthesis in arbitrarily irregular layered media is under development. We will also study the approximation involved in the so-called Rayleigh Ansatz method, or the Aki-Larner method (Aki and Larner, 1970). Aki-Larner method is a wavenumber domain implemented and approximated BIE method. It is much faster than the strict BIE method and therefore can simulate large 3D topography and interface problems. Horike et al. (1990) has applied the method to non-axisymmetric 3D surface structure problems. We will test the accuracy and speed of AL method by comparing it with the strict BIE method (such as Chen's GGRTM method) and incorporate the approximation into our hybrid method.

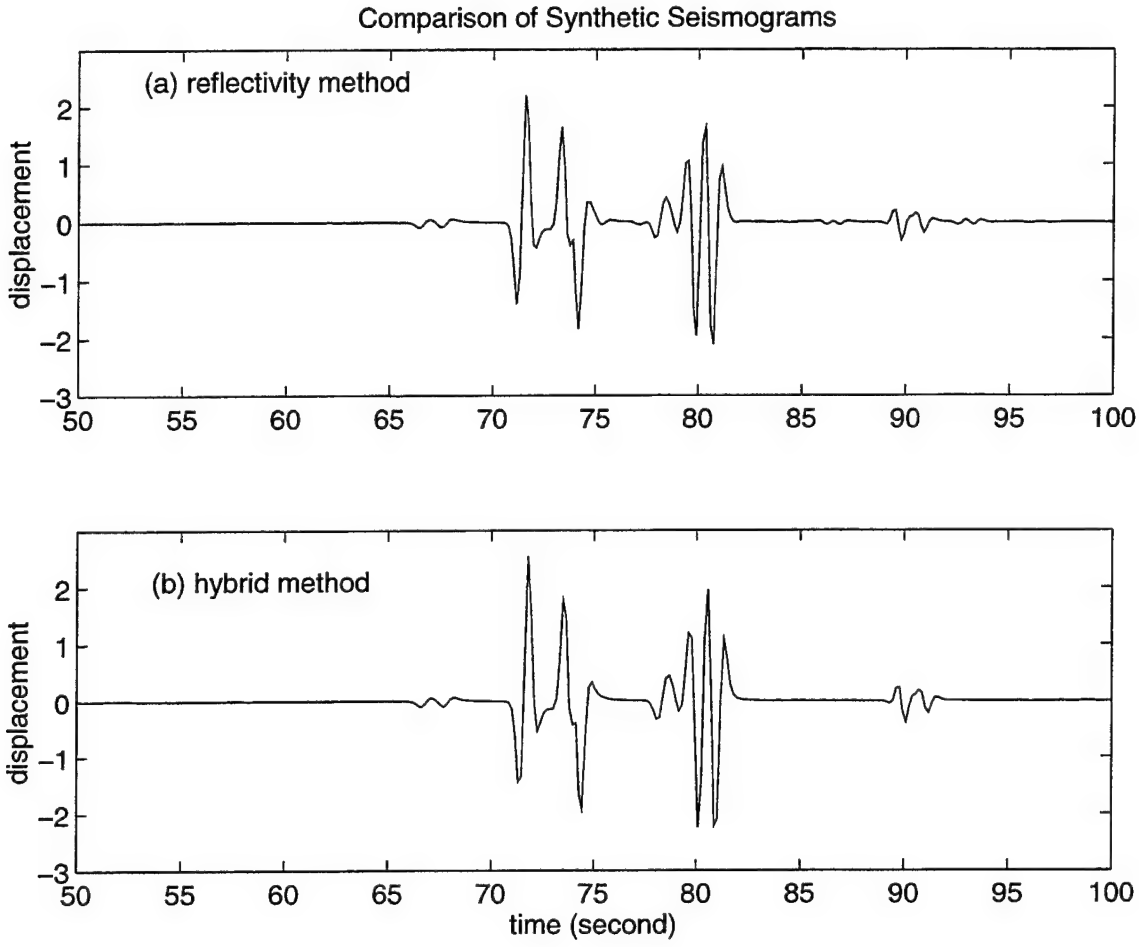

Figure 11: Comparison of synthetic seismograms for a laterally homogeneous layered crustal model. A: synthetic seismogram from a reflectivity method, and B: synthetic seismogram from the hybrid method.

References

[1] Aki, K and K. Larner, 1970, Surface motion of a layered medium having an irregular interface due to incident plane SH waves, *J. Geophys. Res., 75,* 934-954.

[2] Bouchon, M., 1985, A simple, complete numerical solution to the problem of diffraction of SH-waves by an irregular interface, *J. Acoust. Soc. Am., 77,* 1-5.

[3] Bouchon, M., M. Campillo and S. Gaffet, 1989, A boundary integral equation-discrete wavenumber representation method to study wave propagation in multilayered media having irregular interfaces, *Geophysics, 54,* 1134-1140.

[4] Campillo, M., and M. Bouchon, 1985, Synthetic SH-seismograms in a laterally varying medium by the discrete wavenumber method, *Geophys. J. Roy. Astr. Soc., 83,* 307-317.

[5] Campillo, M. and A. Paul, 1992, Influence of lower crustal structure on the early coda of regional seismograms, *J. Geophys. Res., 97,* 3405-3416.

[6] Chen, X.F., 1990, Seismogram synthesis for multi-layered media with irregular interfaces by the global generalized reflection/transmission matrices method - Part I. Theory of 2-D SH case, *Bull. Seismol. Soc. Am., 80,* 1694-1724.

[7] Chen, X.F., 1995, Seismogram synthesis for multi-layered media with irregular interfaces by the global generalized reflection/transmission matrices method - Part II. Applications of 2-D SH case, *Bull. Seismol. Soc. Am., 85,* 1094-1106.

[8] Chen, X.F., 1996, Seismogram synthesis for multi-layered media with irregular interfaces by the global generalized reflection/transmission matrices method - Part III. Theory of 2D P-SV case, *Bull. Seismol. Soc. Am., 86,* 389-405.

[9] Horike, M., H. Uebayashi and Y. Takeuchi, 1990 Seismic response in three-dimensional sedimentary basin due to plane S wave incidence, *J. Phys. Earth, 38,* 261-284.

[10] Sanchez-Sesma, F.J., and M. Campillo, 1991, Diffraction of P, SV and Rayleigh waves by topographic features: a boundary integral formulation, *Bull. Seis. Soc. Am., 81,* 2234-2253.

[11] Wu, R.S., 1994. Wide-angle elastic wave one-way propagation in heterogeneous media and an elastic wave complex-screen method, *J. Geophys. Res.*, **99**, 751-766.

[12] Wu, R.S., 1996, Synthetic seismograms in heterogeneous media by one-return approximation, *Pure and Applied Geophys., 148*, 155-173.

[13] Wu, R.S. and L.J. Huang, 1995, Reflected wave modeling in heterogeneous acoustic media using the de Wolf approximation: *in* S. Hassanzadeh (Ed.), *Mathematical Methods in Geophysical Imaging III*, SPIE Proceedings Series, *2571*, 176-186.

[14] Wu, R.S. and X.B., Xie, 1994, Multi-screen backpropagator for fast 3D elastic prestack migration, *in* S. Hassanzadeh (Ed.), *Mathematical Methods in Geophysical Imaging II*, SPIE Proceedings Series, *2301*, 181-193.

[15] Wu, R.S. T. Lay and X.F. Chen, 1996, Modeling the effects of surface topography on Lg wave propagation by a hybrid method, *Proceedings of the 18th Annual Seismic Research Symposium*, 281-290, PL-TR-96-2153, ADA 313692.

[16] Wu, R.S. S. Jin and X.B. Xie, 1996, Synthetic seismograms in heterogeneous crustal waveguides using screen propagators, *Proceedings of the 18th Annual Seismic Research Symposium*, 291-300, PL-TR-96-2153, ADA 313692.

[17] Xie, X.B. and T. Lay, 1994, The excitation of explosion Lg, a finite-difference investigation, *Bull. Seismol. Soc. Am., 84*, 324-342.

THOMAS AHRENS
SEISMOLOGICAL LABORATORY 252-21
CALIFORNIA INSTITUTE OF TECHNOLOGY
PASADENA, CA 91125

SHELTON ALEXANDER
PENNSYLVANIA STATE UNIVERSITY
DEPARTMENT OF GEOSCIENCES
537 DEIKE BUILDING
UNIVERSITY PARK, PA 16801

RICHARD BARDZELL
ACIS
DCI/ACIS
WASHINGTON, DC 20505

DOUGLAS BAUMGARDT
ENSCO INC.
5400 PORT ROYAL ROAD
SPRINGFIELD, VA 22151

WILLIAM BENSON
NAS/COS
ROOM HA372
2001 WISCONSIN AVE. NW
WASHINGTON, DC 20007

ROBERT BLANDFORD
AFTAC
1300 N. 17TH STREET
SUITE 1450
ARLINGTON, VA 22209-2308

RHETT BUTLER
IRIS
1200 NEW YORK AVE., NW
SUITE 800
WASHINGTON, DC 20005

CATHERINE DE GROOT-HEDLIN
UNIVERSITY OF CALIFORNIA, SAN DIEGO
INSTITUTE OF GEOPHYSICS AND PLANETARY PHYSICS
8604 LA JOLLA SHORES DRIVE
SAN DIEGO, CA 92093

SEAN DORAN
ACIS
DCI/ACIS
WASHINGTON , DC 20505

RICHARD J. FANTEL
BUREAU OF MINES
DEPT OF INTERIOR, BLDG 20
DENVER FEDERAL CENTER
DENVER, CO 80225

RALPH ALEWINE
NTPO
1901 N. MOORE STREET, SUITE 609
ARLINGTON, VA 22209

MUAWIA BARAZANGI
INSTITUTE FOR THE STUDY OF THE CONTINENTS
3126 SNEE HALL
CORNELL UNIVERSITY
ITHACA, NY 14853

T.G. BARKER
MAXWELL TECHNOLOGIES
P.O. BOX 23558
SAN DIEGO, CA 92123

THERON J. BENNETT
MAXWELL TECHNOLOGIES
11800 SUNRISE VALLEY DRIVE SUITE 1212
RESTON, VA 22091

JONATHAN BERGER
UNIVERSITY OF CA, SAN DIEGO
SCRIPPS INSTITUTION OF OCEANOGRAPHY IGPP, 0225
9500 GILMAN DRIVE
LA JOLLA, CA 92093-0225

STEVEN BRATT
NTPO
1901 N. MOORE STREET, SUITE 609
ARLINGTON, VA 22209

LESLIE A. CASEY
DOE
1000 INDEPENDENCE AVE. SW
NN-20
WASHINGTON, DC 20585-0420

STANLEY DICKINSON
AFOSR
110 DUNCAN AVENUE, SUITE B115
BOLLING AFB
WASHINGTON, D.C. 20332-001

DIANE I. DOSER
DEPARTMENT OF GEOLOGICAL SCIENCES
THE UNIVERSITY OF TEXAS AT EL PASO
EL PASO, TX 79968

JOHN FILSON
ACIS/TMG/NTT
ROOM 6T11 NHB
WASHINGTON, DC 20505

MARK D. FISK
MISSION RESEARCH CORPORATION
735 STATE STREET
P.O. DRAWER 719
SANTA BARBARA, CA 93102-0719

LORI GRANT
MULTIMAX, INC.
311C FOREST AVE. SUITE 3
PACIFIC GROVE, CA 93950

I. N. GUPTA
MULTIMAX, INC.
1441 MCCORMICK DRIVE
LARGO, MD 20774

JAMES HAYES
NSF
4201 WILSON BLVD., ROOM 785
ARLINGTON, VA 22230

MICHAEL HEDLIN
UNIVERSITY OF CALIFORNIA, SAN DIEGO
SCRIPPS INSTITUTION OF OCEANOGRAPHY IGPP, 0225
9500 GILMAN DRIVE
LA JOLLA, CA 92093-0225

EUGENE HERRIN
SOUTHERN METHODIST UNIVERSITY
DEPARTMENT OF GEOLOGICAL SCIENCES
DALLAS, TX 75275-0395

VINDELL HSU
HQ/AFTAC/TTR
1030 S. HIGHWAY A1A
PATRICK AFB, FL 32925-3002

RONG-SONG JIH
PHILLIPS LABORATORY
EARTH SCIENCES DIVISION
29 RANDOLPH ROAD
HANSCOM AFB, MA 01731-3010

LAWRENCE LIVERMORE NATIONAL LABORATORY
ATTN: TECHNICAL STAFF (PLS ROUTE)
PO BOX 808, MS L-200
LIVERMORE, CA 94551

LAWRENCE LIVERMORE NATIONAL LABORATORY
ATTN: TECHNICAL STAFF (PLS ROUTE)
PO BOX 808, MS L-221
LIVERMORE, CA 94551

ROBERT GEIL
DOE
PALAIS DES NATIONS, RM D615
GENEVA 10, SWITZERLAND

HENRY GRAY
SMU STATISTICS DEPARTMENT
P.O. BOX 750302
DALLAS, TX 75275-0302

DAVID HARKRIDER
PHILLIPS LABORATORY
EARTH SCIENCES DIVISION
29 RANDOLPH ROAD
HANSCOM AFB, MA 01731-3010

THOMAS HEARN
NEW MEXICO STATE UNIVERSITY
DEPARTMENT OF PHYSICS
LAS CRUCES, NM 88003

DONALD HELMBERGER
CALIFORNIA INSTITUTE OF TECHNOLOGY
DIVISION OF GEOLOGICAL & PLANETARY SCIENCES
SEISMOLOGICAL LABORATORY
PASADENA, CA 91125

ROBERT HERRMANN
ST. LOUIS UNIVERSITY
DEPARTMENT OF EARTH & ATMOSPHERIC SCIENCES
3507 LACLEDE AVENUE
ST. LOUIS, MO 63103

ANTHONY IANNACCHIONE
BUREAU OF MINES
COCHRANE MILL ROAD
PO BOX 18070
PITTSBURGH, PA 15236-9986

THOMAS JORDAN
MASSACHUSETTS INSTITUTE OF TECHNOLOGY
EARTH, ATMOSPHERIC & PLANETARY SCIENCES
77 MASSACHUSETTS AVENUE, 54-918
CAMBRIDGE, MA 02139

LAWRENCE LIVERMORE NATIONAL LABORATORY
ATTN: TECHNICAL STAFF (PLS ROUTE)
PO BOX 808, MS L-207
LIVERMORE, CA 94551

LAWRENCE LIVERMORE NATIONAL LABORATORY
ATTN: TECHNICAL STAFF (PLS ROUTE)
LLNL
PO BOX 808, MS L-175
LIVERMORE, CA 94551

LAWRENCE LIVERMORE NATIONAL LABORATORY
ATTN: TECHNICAL STAFF (PLS ROUTE)
PO BOX 808, MS L-208
LIVERMORE, CA 94551

LAWRENCE LIVERMORE NATIONAL LABORATORY
ATTN: TECHNICAL STAFF (PLS ROUTE)
PO BOX 808, MS L-195
LIVERMORE, CA 94551

THORNE LAY
UNIVERSITY OF CALIFORNIA, SANTA CRUZ
EARTH SCIENCES DEPARTMENT
EARTH & MARINE SCIENCE BUILDING
SANTA CRUZ, CA 95064

DONALD A. LINGER
DNA
6801 TELEGRAPH ROAD
ALEXANDRIA, VA 22310

LOS ALAMOS NATIONAL LABORATORY
ATTN: TECHNICAL STAFF (PLS ROUTE)
PO BOX 1663, MS F665
LOS ALAMOS, NM 87545

LOS ALAMOS NATIONAL LABORATORY
ATTN: TECHNICAL STAFF (PLS ROUTE)
PO BOX 1663, MS C335
LOS ALAMOS, NM 87545

KEITH MCLAUGHLIN
MAXWELL TECHNOLOGIES
P.O. BOX 23558
SAN DIEGO, CA 92123

RICHARD MORROW
USACDA/IVI
320 21ST STREET, N.W.
WASHINGTON, DC 20451

JAMES NI
NEW MEXICO STATE UNIVERSITY
DEPARTMENT OF PHYSICS
LAS CRUCES, NM 88003

PACIFIC NORTHWEST NATIONAL LABORATORY
ATTN: TECHNICAL STAFF (PLS ROUTE)
PO BOX 999, MS K6-48
RICHLAND, WA 99352

LAWRENCE LIVERMORE NATIONAL LABORATORY
ATTN: TECHNICAL STAFF (PLS ROUTE)
PO BOX 808, MS L-202
LIVERMORE, CA 94551

LAWRENCE LIVERMORE NATIONAL LABORATORY
ATTN: TECHNICAL STAFF (PLS ROUTE)
PO BOX 808, MS L-205
LIVERMORE, CA 94551

ANATOLI L. LEVSHIN
DEPARTMENT OF PHYSICS
UNIVERSITY OF COLORADO
CAMPUS BOX 390
BOULDER, CO 80309-0309

LOS ALAMOS NATIONAL LABORATORY
ATTN: TECHNICAL STAFF (PLS ROUTE)
PO BOX 1663, MS F659
LOS ALAMOS, NM 87545

LOS ALAMOS NATIONAL LABORATORY
ATTN: TECHNICAL STAFF (PLS ROUTE)
PO BOX 1663, MS D460
LOS ALAMOS, NM 87545

GARY MCCARTOR
SOUTHERN METHODIST UNIVERSITY
DEPARTMENT OF PHYSICS
DALLAS, TX 75275-0395

BRIAN MITCHELL
DEPARTMENT OF EARTH & ATMOSPHERIC SCIENCES
ST. LOUIS UNIVERSITY
3507 LACLEDE AVENUE
ST. LOUIS, MO 63103

JOHN MURPHY
MAXWELL TECHNOLOGIES
11800 SUNRISE VALLEY DRIVE SUITE 1212
RESTON, VA 22091

JOHN ORCUTT
INSTITUTE OF GEOPHYSICS AND PLANETARY PHYSICS
UNIVERSITY OF CALIFORNIA, SAN DIEGO
LA JOLLA, CA 92093

PACIFIC NORTHWEST NATIONAL LABORATORY
ATTN: TECHNICAL STAFF (PLS ROUTE)
PO BOX 999, MS K7-34
RICHLAND, WA 99352

PACIFIC NORTHWEST NATIONAL LABORATORY
ATTN: TECHNICAL STAFF (PLS ROUTE)
PO BOX 999, MS K6-40
RICHLAND, WA 99352

PACIFIC NORTHWEST NATIONAL LABORATORY
ATTN: TECHNICAL STAFF (PLS ROUTE)
PO BOX 999, MS K5-12
RICHLAND, WA 99352

KEITH PRIESTLEY
DEPARTMENT OF EARTH SCIENCES
UNIVERSITY OF CAMBRIDGE
MADINGLEY RISE, MADINGLEY ROAD
CAMBRIDGE, CB3 OEZ UK

PAUL RICHARDS
COLUMBIA UNIVERSITY
LAMONT-DOHERTY EARTH OBSERVATORY
PALISADES, NY 10964

CHANDAN SAIKIA
WOOODWARD-CLYDE FEDERAL SERVICES
566 EL DORADO ST., SUITE 100
PASADENA, CA 91101-2560

SANDIA NATIONAL LABORATORY
ATTN: TECHNICAL STAFF (PLS ROUTE)
DEPT. 5791
MS 0567, PO BOX 5800
ALBUQUERQUE, NM 87185-0567

SANDIA NATIONAL LABORATORY
ATTN: TECHNICAL STAFF (PLS ROUTE)
DEPT. 5704
MS 0655, PO BOX 5800
ALBUQUERQUE, NM 87185-0655

THOMAS SERENO JR.
SCIENCE APPLICATIONS INTERNATIONAL
CORPORATION
10260 CAMPUS POINT DRIVE
SAN DIEGO, CA 92121

ROBERT SHUMWAY
410 MRAK HALL
DIVISION OF STATISTICS
UNIVERSITY OF CALIFORNIA
DAVIS, CA 95616-8671

DAVID SIMPSON
IRIS
1200 NEW YORK AVE., NW
SUITE 800
WASHINGTON, DC 20005

PACIFIC NORTHWEST NATIONAL LABORATORY
ATTN: TECHNICAL STAFF (PLS ROUTE)
PO BOX 999, MS K6-84
RICHLAND, WA 99352

FRANK PILOTTE
HQ/AFTAC/TT
1030 S. HIGHWAY A1A
PATRICK AFB, FL 32925-3002

JAY PULLI
BBN
1300 NORTH 17TH STREET
ROSSLYN, VA 22209

DAVID RUSSELL
HQ AFTAC/TTR
1030 SOUTH HIGHWAY A1A
PATRICK AFB, FL 32925-3002

SANDIA NATIONAL LABORATORY
ATTN: TECHNICAL STAFF (PLS ROUTE)
DEPT. 5704
MS 0979, PO BOX 5800
ALBUQUERQUE, NM 87185-0979

SANDIA NATIONAL LABORATORY
ATTN: TECHNICAL STAFF (PLS ROUTE)
DEPT. 9311
MS 1159, PO BOX 5800
ALBUQUERQUE, NM 87185-1159

SANDIA NATIONAL LABORATORY
ATTN: TECHNICAL STAFF (PLS ROUTE)
DEPT. 5736
MS 0655, PO BOX 5800
ALBUQUERQUE, NM 87185-0655

AVI SHAPIRA
SEISMOLOGY DIVISION
THE INSTITUTE FOR PETROLEUM RESEARCH AND
GEOPHYSICS
P.O.B. 2286, NOLON 58122 ISRAEL

MATTHEW SIBOL
ENSCO, INC.
445 PINEDA COURT
MELBOURNE, FL 32940

JEFFRY STEVENS
MAXWELL TECHNOLOGIES
P.O. BOX 23558
SAN DIEGO, CA 92123

BRIAN SULLIVAN
BOSTON COLLEGE
INSITUTE FOR SPACE RESEARCH
140 COMMONWEALTH AVENUE
CHESTNUT HILL, MA 02167

NAFI TOKSOZ
EARTH RESOURCES LABORATORY, M.I.T.
42 CARLTON STREET, E34-440
CAMBRIDGE, MA 02142

GREG VAN DER VINK
IRIS
1200 NEW YORK AVE., NW
SUITE 800
WASHINGTON, DC 20005

TERRY WALLACE
UNIVERSITY OF ARIZONA
DEPARTMENT OF GEOSCIENCES
BUILDING #77
TUCSON, AZ 85721

JAMES WHITCOMB
NSF
NSF/ISC OPERATIONS/EAR-785
4201 WILSON BLVD., ROOM785
ARLINGTON, VA 22230

JIAKANG XIE
COLUMBIA UNIVERSITY
LAMONT DOHERTY EARTH OBSERVATORY
ROUTE 9W
PALISADES, NY 10964

OFFICE OF THE SECRETARY OF DEFENSE
DDR&E
WASHINGTON, DC 20330

TACTEC
BATTELLE MEMORIAL INSTITUTE
505 KING AVENUE
COLUMBUS, OH 43201 (FINAL REPORT)

PHILLIPS LABORATORY
ATTN: GPE
29 RANDOLPH ROAD
HANSCOM AFB, MA 01731-3010

PHILLIPS LABORATORY
ATTN: PL/SUL
3550 ABERDEEN AVE SE
KIRTLAND, NM 87117-5776 (2 COPIES)

DAVID THOMAS
ISEE
29100 AURORA ROAD
CLEVELAND, OH 44139

LAWRENCE TURNBULL
ACIS
DCI/ACIS
WASHINGTON, DC 20505

FRANK VERNON
UNIVERSITY OF CALIFORNIA, SAN DIEGO
SCRIPPS INSTITUTION OF OCEANOGRAPHY IGPP, 0225
9500 GILMAN DRIVE
LA JOLLA, CA 92093-0225

DANIEL WEILL
NSF
EAR-785
4201 WILSON BLVD., ROOM 785
ARLINGTON, VA 22230

RU SHAN WU
UNIVERSITY OF CALIFORNIA SANTA CRUZ
EARTH SCIENCES DEPT.
1156 HIGH STREET
SANTA CRUZ, CA 95064

JAMES E. ZOLLWEG
BOISE STATE UNIVERSITY
GEOSCIENCES DEPT.
1910 UNIVERSITY DRIVE
BOISE, ID 83725

DEFENSE TECHNICAL INFORMATION CENTER
8725 JOHN J. KINGMAN ROAD
FT BELVOIR, VA 22060-6218 (2 COPIES)

PHILLIPS LABORATORY
ATTN: GPBP
29 RANDOLPH ROAD
HANSCOM AFB, MA 01731-3010

PHILLIPS LABORATORY
ATTN: RESEARCH LIBRARY/TL
5 WRIGHT STREET
HANSCOM AFB, MA 01731-3004